Acta Radiologica Open
6(11) 1–9

DOI: 10.1177/2058460117729186
journals.sagepub.com/home/arr
SAGE

Influence of longitudinal position on the evolution of steady-state signal in cardiac cine balanced steady-state free precession imaging

Tyler J Spear[1], Tori A Stromp[1,2], Steve W Leung[1,3] and Moriel H Vandsburger[1,2,4]

Abstract

Background: Emerging quantitative cardiac magnetic resonance imaging (CMRI) techniques use cine balanced steady-state free precession (bSSFP) to measure myocardial signal intensity and probe underlying physiological parameters. This correlation assumes that steady-state is maintained uniformly throughout the heart in space and time.

Purpose: To determine the effects of longitudinal cardiac motion and initial slice position on signal deviation in cine bSSFP imaging by comparing two-dimensional (2D) and three-dimensional (3D) acquisitions.

Material and Methods: Nine healthy volunteers completed cardiac MRI on a 1.5-T scanner. Short axis images were taken at six slice locations using both 2D and 3D cine bSSFP. 3D acquisitions spanned two slices above and below selected slice locations. Changes in myocardial signal intensity were measured across the cardiac cycle and compared to longitudinal shortening.

Results: For 2D cine bSSFP, 46% ± 9% of all frames and 84% ± 13% of end-diastolic frames remained within 10% of initial signal intensity. For 3D cine bSSFP the proportions increased to 87% ± 8% and 97% ± 5%. There was no correlation between longitudinal shortening and peak changes in myocardial signal. The initial slice position significantly impacted peak changes in signal intensity for 2D sequences ($P < 0.001$).

Conclusion: The initial longitudinal slice location significantly impacts the magnitude of deviation from steady-state in 2D cine bSSFP that is only restored at the center of a 3D excitation volume. During diastole, a transient steady-state is established similar to that achieved with 3D cine bSSFP regardless of slice location.

Keywords
3D, magnetic resonance imaging (MRI), heart, steady-state imaging, cardiac motion

Date received: 28 July 2017; accepted: 8 August 2017

Introduction

Balanced steady-state free precession (bSSFP) imaging (1) has become the clinical standard technique for cardiac magnetic resonance imaging (CMRI) due to excellent contrast between myocardial tissue and the adjacent ventricular blood pool (2,3). Recently, several studies have noted that changes in tissue structure due to edema (4,5) and fibrosis (6) generate quantifiable changes in myocardial signal intensity. While these techniques often rely only on end-diastolic images, other techniques that require accurate and consistent bSSFP signal throughout an entire cardiac cycle, such

[1]Saha Cardiovascular Research Center, University of Kentucky, Lexington, KY, USA
[2]Department of Physiology, University of Kentucky, Lexington, KY, USA
[3]Gill Heart Institute, University of Kentucky, Lexington, KY, USA
[4]Department of Bioengineering, University of California, Berkeley, CA, USA

Corresponding author:
Moriel H Vandsburger, 419 Hearst Memorial Mining Building, UC Berkeley, Bioengineering, Berkeley, CA 94707, USA.
Email: moriel@berkeley.edu

as mapping of native-T1 relaxation times (7) and blood oxygen level dependent (BOLD) imaging (8), are increasingly used for quantitative CMRI. Although the underlying mechanisms of cine bSSFP imaging are well modeled and understood (9,10), it has been shown that measured signal intensity values in the myocardium diverge substantially from the predicted signal intensities (11). While some of the discrepancies can be attributed to imperfections in magnetic field homogeneity, non-ideal pulse profiles, magnetization transfer (MT), and off-resonance effects due to proximity to other organs such as lungs (11), Goldfarb et al. previously demonstrated that changes in myocardial signal intensity throughout the cardiac cycle exhibit a cyclical pattern that results in a transient steady-state in the myocardium (12). Cardiac motion even in the presence of gating has long been shown to impact signal intensity and relaxation times (13). However, previous studies have only explored such factors in a single mid-ventricular imaging slice without taking into account the complex three-dimensional (3D) motion of the heart during the cardiac cycle. The contributions of the initial longitudinal slice position of axial imaging slices and of longitudinal shortening during the cardiac cycle to the evolution of steady-state myocardial signal in two-dimensional (2D) cine bSSFP remain unexplored. As quantitative CMRI methods are increasingly applied to whole heart imaging, it is important to fully understand the factors that contribute to changes in signal evolution that may confound measurements derived from such methods.

The purpose of this study was to examine the impact of the initial longitudinal slice position within the heart and peak longitudinal shortening during contraction on the evolution of steady-state magnetization in 2D cine bSSFP by comparison to 3D volume (slab) cine bSSFP. We hypothesized that cyclical deviation from steady-state signal in 2D cine bSSFP is a function of the initial longitudinal position of the axial imaging slice. We further hypothesized that using 3D cine bSSFP sequences can eliminate the impact of slice location on deviation from steady-state signal.

Material and Methods

Scan protocol

Nine healthy adult male volunteers with no history of tobacco use or cardiovascular disease (mean age = 25.7 years, age range = 23–29 years) completed CMRI on a 1.5 T Siemens Aera scanner (Erlangen, Germany) using an 18-channel body coil and 12-channel spine coil. Additional system specifications included gradient strength of 45 mT/m and slew rate of 200 T/m/s. The local Institutional Review Board approved the study. All participants were informed and consented prior to scanning. Localizing scans, including a four-chamber cine, were performed to acquire a single short axis stack spanning from left ventricular base to apex consisting of nine 8-mm thick slices. Starting at the most basal position of the left ventricle in which the ventricular myocardium was contiguous throughout the cardiac cycle, every other slice was used as the center of a 3D cine bSSFP acquisition (slab) consisting of six 8-mm thick slices across a total of three slabs (Fig. 1). Additional scan parameters include: TR/TE = 3.4/1.46 ms, field of view (FOV) = 260×260 mm^2, flip angle = 50°, matrix = 256×256, in-plane spatial resolution = 1×1 mm^2, number of averages = 1, acceleration factor = 2, phase sampling = 75%. Prospective electrocardiogram triggering was used. In parallel, a stack of corresponding 2D cine bSSFP acquisitions were performed at slice locations corresponding to the same location as the two center slices of each slab

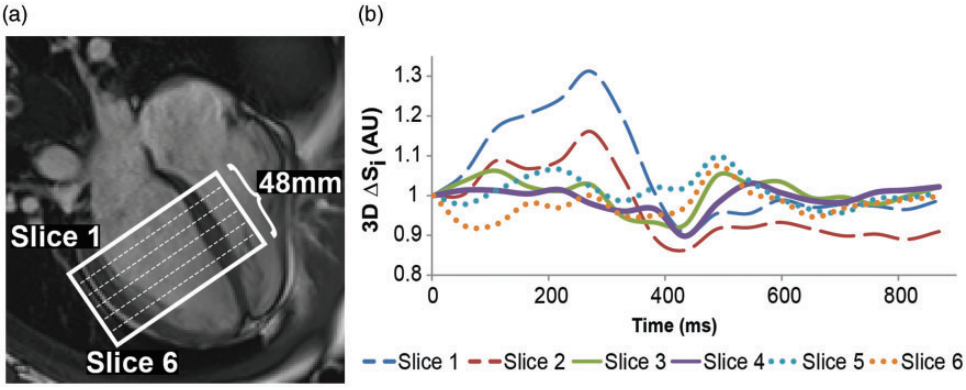

Fig. 1. (a) Long axis, four-chamber end-diastolic image of the heart with a superimposed schematic of the slab and slice architecture for one representative slab. (b) Normalized signal intensity waveforms for all six slices in one 3D slab are shown throughout the entire cardiac cycle. Solid lines represent the middle two slices (slice 3 and 4) which were used for all other analyses of 3D images.

(Fig. 1). All acquisition parameters were maintained for 2D imaging except TR/TE (3.2/1.2 ms). All acquisitions were single breath-hold acquisitions across both protocols. The mean scan time for a single 3D slab was 21 s and for a single 2D slice was 9 s. Total scan time for each individual was roughly 30 min.

Image analysis

All data analysis was performed using custom written software in Matlab version 2013a (Mathworks, Natick, MA, USA). Epicardial and endocardial borders were defined for each cardiac phase using a custom feature tracking algorithm (14) and the average myocardial signal intensity was measured for both 2D and 3D acquisitions. All myocardial voxels within the two borders were used to calculate a mean signal intensity. The dynamic change from the initial myocardial signal (S_0) was defined as $\Delta S_i = S_i/S_0$, where S_i is the average myocardial signal intensity at each cardiac phase *i*. A single cardiac phase was identified as maintaining steady-state if the signal intensity S_i was within 10% of S_0. For each slice and acquisition mode, the deviation from steady-state was quantified by measuring the ratio of cardiac phases with changes in signal intensity greater than 10% to the total number of phases in that acquisition. Identical analysis was performed over diastolic phases representing the last 30% of the cardiac cycle. Temporal information was gathered from trigger time and cardiac interval recorded at the time of scan.

Separately, a single observer used the same custom feature tracking algorithm (14) to define the apex and mitral valve insertion points on each phase of a four-chamber cine series for each participant. The mitral plane was defined by the line between these connection points. The distance from the midpoint of this mitral line to the apex was used to define the longitudinal length (L) of the heart as described in (15). Longitudinal shortening was defined as $\Delta L_i = L_0 - L_i$ for each phase *i*. In order to reduce variability in the definition of L_0 and L_i, two observers defined the apex and mitral valve plane on the same four-chamber cine images in the first phase and at end systole. Average peak ΔL_i between observers was used for analysis. End-systolic images were overlaid on the first frame and the distance between the points defining the apex were used to define displacement of the apex. This process was repeated using the midpoints defined from the mitral valve insertion points. Local signal maxima corresponding to systole and the end of diastolic filling were identified from each ΔS_i waveform for both 2D and 3D imaging. Signal maxima were compared to the initial slice location, measured from the mitral plane, and to maximum ΔL_i for each individual.

Statistical analysis

Statistical analysis was completed using IBM SPSS Statistics Version 22 (IBM Corp, Armonk, NY, USA). Student's t-tests were used to compare ratios of total and diastolic phases within 10% of S_0 as well as maximum signal changes between 2D and 3D acquisitions. Linear regressions were used to compare maximum ΔS_i at both end systole and late diastolic filling against slice location. Pearson correlations were used to compare maximum ΔS_i at both end systole and late diastolic filling. Data are presented as mean ± standard deviation. For all comparisons, $P < 0.05$ was considered significant.

Results

Steady-state characteristics within a 3D slab

Examination of ΔS_i across all slices within 3D slabs revealed preservation of steady-state magnetization predominantly within the two middle slices (slices 3 and 4). Representative ΔS_i waveforms for all slices within a 3D slab centered at the mid-ventricle are shown in Fig. 1 and demonstrate substantial deviation from steady-state values in outer slices. In parallel, image quality was significantly reduced in slices at the borders of the 3D volume as shown in Fig. 2. Noticeable artifacts were observed in the anterior and lateral walls, and blurring was observed in the septum and inferior wall in images acquired at slice positions 1, 2, 5, and 6 within a 3D volume. Based on these findings, all comparisons of signal evolution were performed between 2D cine bSSFP and corresponding 3D data when the slice was acquired at the center of the 3D slab (slices 3 and 4).

Signal evolution

Sample images at end-diastole, peak systole, and late diastolic filling acquired with 2D and 3D cine bSSFP are shown in Fig. 3. Corresponding ΔS_i waveforms demonstrate substantial changes in myocardial signal intensity in 2D cine bSSFP throughout the majority of the cardiac cycle that are not present in the 3D acquisition. Across all individuals and slices, nearly all cardiac phases demonstrated myocardial signal intensity within 10% of initial values for 3D cine bSSFP acquisitions (Fig. 4). In comparison, corresponding measurements for images acquired with 2D cine bSSFP were preserved in approximately half of cardiac phases (Fig. 4). During the last 30% of the cardiac cycle, both 2D and 3D bSSFP acquisitions result in a high percentage of phases with signal intensity within 10% of initial signal intensity (Fig. 4). However, this value was significantly higher in 3D

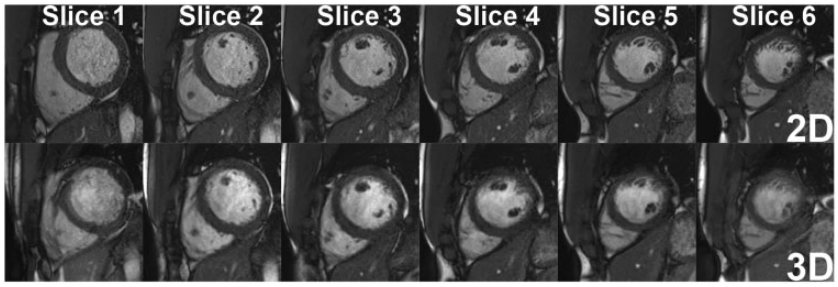

Fig. 2. Representative end-diastolic images acquired with 2D and 3D cine bSSFP for all slices in a 3D slab as shown on the long axis image in Fig. 1. 3D images come from a single slab acquisition and display artifacts and reduction of image quality in outer slices (1, 2, 5, and 6) when compared to corresponding 2D cine bSSFP images.

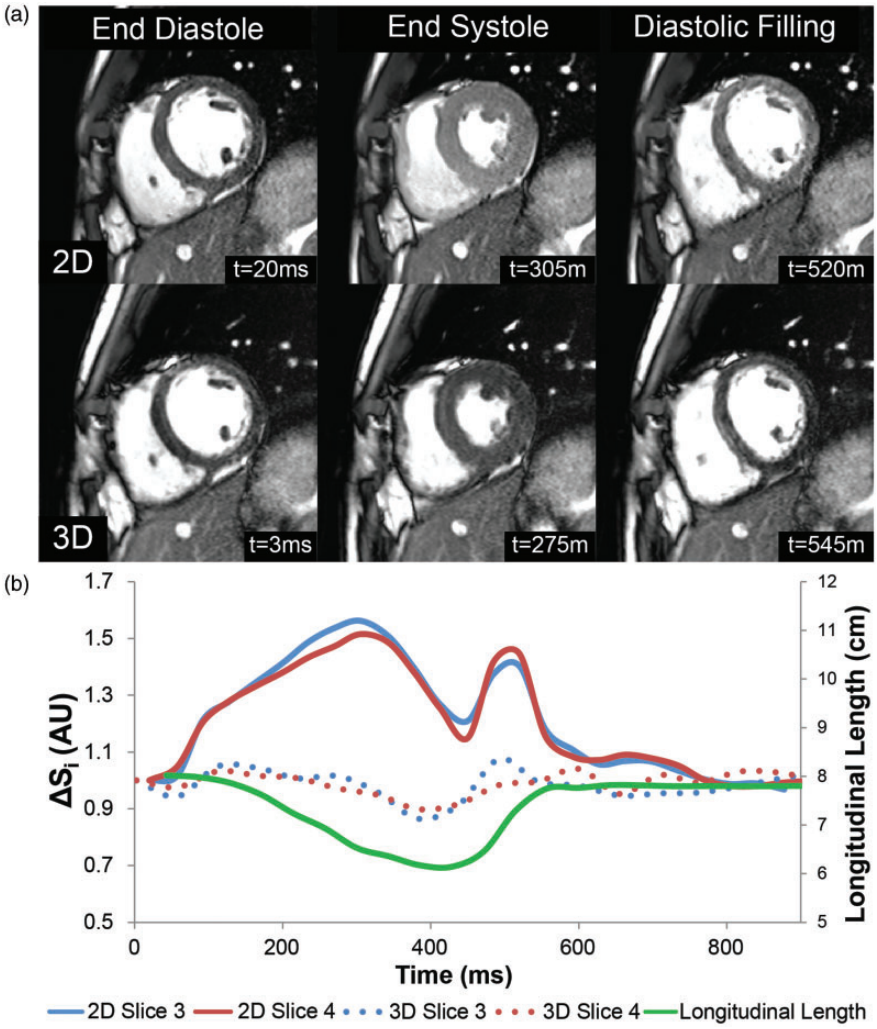

Fig. 3. (a) Representative mid-ventricular images at end-diastolic (initial phase), end-systolic, and diastolic filling phases of the cardiac cycle acquired at the same slice position using 2D (top) and 3D acquisitions (bottom). All images are windowed and leveled identically in order to reveal changes in myocardial signal intensity. Images acquired using 2D cine bSSFP demonstrated substantially increased myocardial signal intensity at end-systole and during diastolic filling compared to end-diastole. In contrast, myocardial signal intensity is similar at end-diastole, peak systole, and during diastolic filling when images are acquired with 3D cine bSSFP. (b) Normalized signal intensity waveforms from 2D and 3D acquisitions for the slice shown in (a) and the adjacent slice at the center of the 3D slab demonstrate the degree of deviation from steady-state in 2D cine bSSFP as a function of cardiac phase. Despite significant deviation from initial values, myocardial signal intensity returns to steady-state values by the conclusion of the cardiac cycle in 2D cine bSSFP. The longitudinal length (L) during the cardiac cycle in this individual is plotted on the same time scale for purposes of comparison.

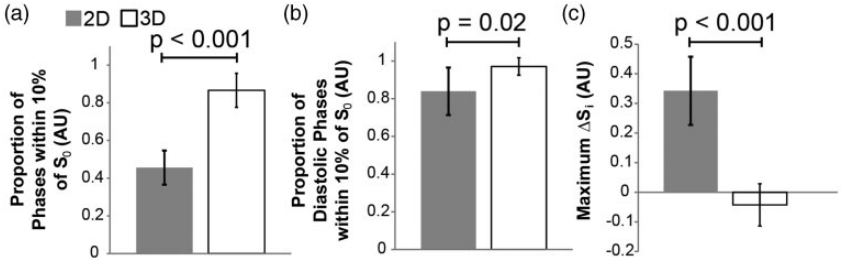

Fig. 4. (a) The proportion of total cardiac phases with myocardial signal intensity within 10% of the initial signal intensity is significantly higher in 3D cine bSSFP compared to 2D cine bSSFP acquisitions. (b) A higher proportion of cardiac phases demonstrates myocardial signal intensity within 10% of initial signal intensity in 2D cine bSSFP when examination is limited to only the last 30% of the cardiac cycle (diastolic phases). However, there remains a statistically significant difference between 2D and 3D cine bSSFP acquisitions. (c) Maximum ΔS_i across the entire cardiac cycle is significantly greater in 2D compared to 3D cine bSSFP. Error bars represent one standard deviation.

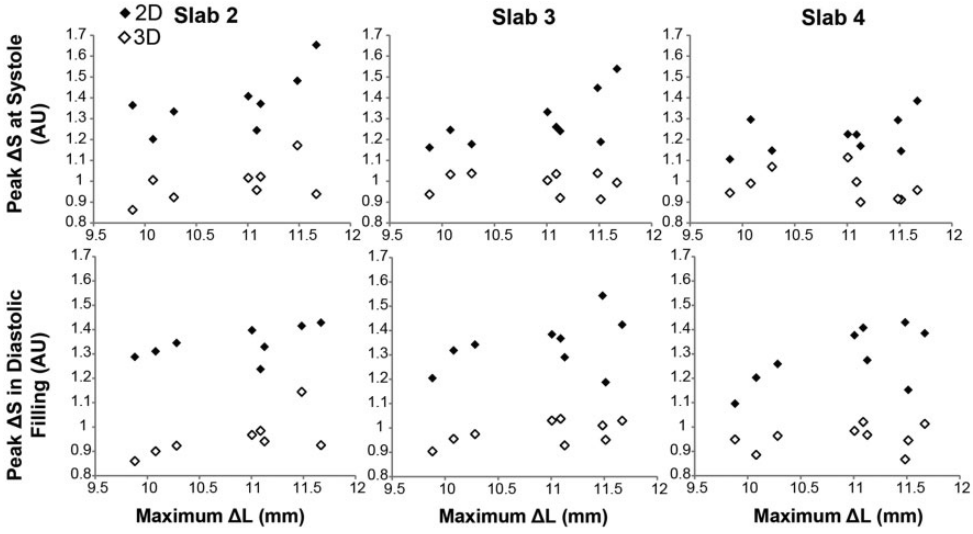

Fig. 5. Magnitude of longitudinal shortening does not influence deviation from steady-state signal intensity when accounting for initial slice position. Peak systolic (top) and diastolic (bottom) changes in normalized myocardial signal intensity are shown as a function of maximum longitudinal shortening (ΔL) for both 2D and 3D cine bSSFP. Analysis using Pearson correlations (Table 1) revealed no meaningful correlation between maximal longitudinal shortening and peak signal changes when the initial longitudinal position of the 2D imaging slice was taken into account.

acquisitions compared to 2D cine bSSFP (Fig. 4). The maximum deviation from the initial signal intensity was uniformly significantly higher in 2D acquisitions compared to corresponding 3D acquisitions (Fig. 4).

Longitudinal shortening and slice location

Comparison of the maximum change in signal intensity at both peak systole and during diastolic filling to the maximum change in length of the left ventricle revealed no significant correlation when accounting for the initial longitudinal position of the imaging slice (Fig. 5), though 2D imaging at peak systole was trending towards significant ($P = 0.07$). Corresponding Pearson correlation statistics are found in Table 1. The average maximal longitudinal displacement of the mitral plane was 9.09 ± 1.51 mm, compared to 3.60 ± 1.29 mm at the apex, as measured on the four-chamber cine. The range of ΔL_i across all patients was 1.79 mm. The initial longitudinal slice position within the heart, measured as the distance from the mitral valve, demonstrated a significant and negative correlation ($P < 0.001$) with peak systolic ΔS_i in 2D cine bSSFP (Fig. 6). The average difference in peak systolic ΔS_i between the most basal and apical slices was 0.221 ± 0.163 (AU). In contrast, no correlation was found when images were acquired using 3D cine bSSFP (Fig. 6). For both 2D and 3D cine bSSFP, the peak ΔS_i during the period of diastolic

Table 1. Pearson correlation statistics for longitudinal shortening and maximum signal changes (maximum ΔL_i vs. peak ΔS_i)

		Pearson rho (*p*)		
	Acquisition	Slab 2	Slab 3	Slab 4
Systole	2D	0.669 (0.070)	0.652 (0.057)	0.445 (0.230)
	3D	0.532 (0.175)	−0.116 (0.765)	−0.318 (0.404)
Diastolic filling	2D	0.559 (0.150)	0.419 (0.261)	0.609 (0.082)
	3D	0.639 (0.088)	0.555 (0.121)	0.230 (0.552)

The Pearson coefficient (rho) represents the strength of correlation, while the *P* value in parentheses represents the statistical significance of the observed correlation.

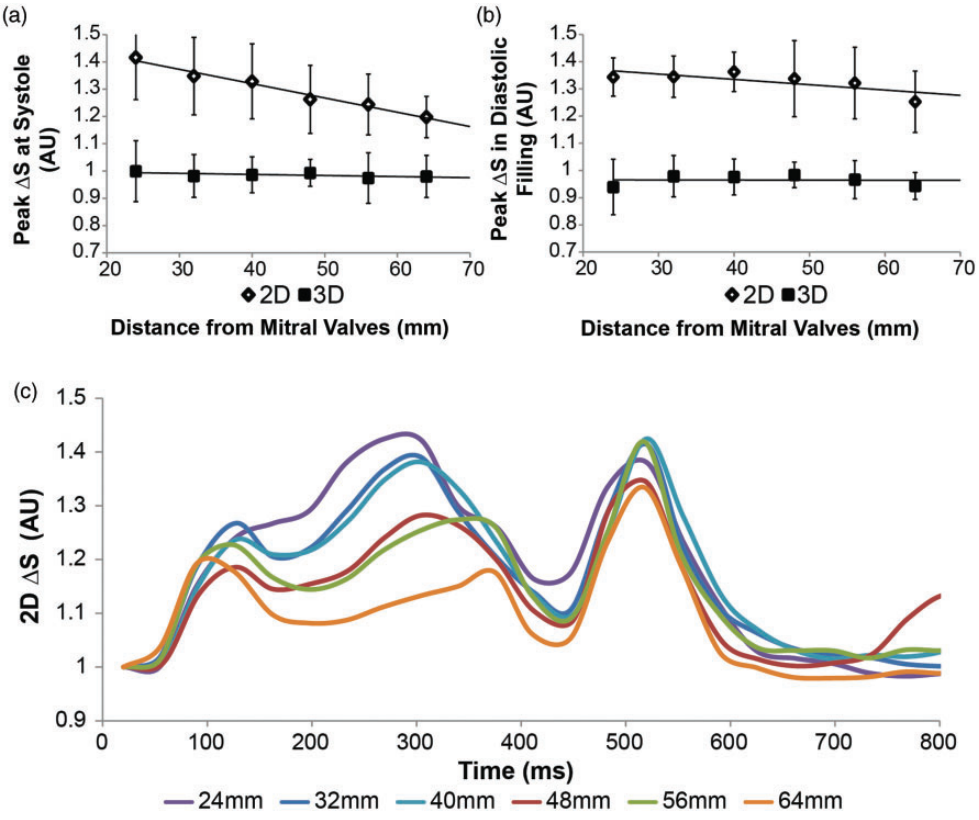

Fig. 6. The maximum change in myocardial signal intensity at peak systole is correlated to the initial longitudinal position of the imaging slice in 2D cine bSSFP. (a) The average peak change in myocardial signal intensity at systole is greatest at the base of the left ventricle and diminishes significantly towards the apex in 2D cine bSSFP ($P < 0.005$ for linear regression analysis). For purposes of comparison, the corresponding measures using 3D cine bSSFP demonstrate maintained steady-state values at peak systole across all initial slice positions. (b) During diastolic filling, the peak signal change in 2D cine bSSFP is uniformly elevated across all initial slice positions ($P = 0.068$). (c) Representative waveforms of normalized myocardial signal intensity acquired with 2D cine bSSFP for six slices across heart demonstrate the gradient in peak systolic signal change with similar peak diastolic signal change. The distance (mm) from the mitral valve for each slice measured at end-diastole is shown in the legend. Error bars indicate one standard deviation. Linear fit statistics can be found in Table 2.

filling did not demonstrate a significant correlation with slice position (Fig. 6, Table 2). Representative ΔS_i waveforms for multiple 2D acquisitions at incremental slice positions demonstrate the gradient from base to apex in peak systolic ΔS_i and consistent peak ΔS_i during diastolic filling (Fig. 6).

Discussion

In this study, we examined the influence of initial longitudinal slice position and global longitudinal shortening in modulating steady-state signal evolution in 2D cine bSSFP. Our findings revealed that the initial

Table 2. Linear regression statistics for maximum signal changes and slice locations (maximum ΔS_i vs. slice location).

	Systole		Diastolic filling	
	2D	3D	2D	3D
Slope (AU/mm)	−0.005	0.000	−0.002	0.001
Y-int (AU)	1.53	0.987	1.415	0.948
R	0.266	0.003	0.066	0.012
P value	<0.001	0.708	0.068	0.449

longitudinal slice position plays a determining role in the peak deviation from steady-state during systole in 2D cine bSSFP. In contrast, the magnitude of global longitudinal shortening does not appear to influence the deviation from steady-state. Importantly, despite significant deviations from steady-state early in the cardiac cycle, the majority of 2D acquisitions had returned to initial steady-state signal intensity by the end of diastole.

While we found no correlation between ΔS_i and global longitudinal shortening, the significant impact of the initial slice location in 2D cine bSSFP imaging implies that slice-specific through-plane motion may contribute to patterns of deviation from steady-state. During the cardiac cycle, the base of the heart undergoes greater translation compared to the apex, which displays more torsional motion (16). In a given slice, the proportion of non-steady-state spins throughout the cardiac cycle will be most impacted by the magnitude of through-plane motion. This pattern of through-plane motion likely underlies the gradient in maximum deviation from steady-state observed in this study.

Increasingly, bSSFP approaches are being implemented for quantitative CMRI techniques including imaging of myocardial perfusion (17,18), diffusion-weighted imaging (19), and for measurement of ventricular T1 (20) and T2 (21) relaxation times. In addition, several studies have examined the utility of atrial signal intensities on cine bSSFP imaging for surgical planning with catheter ablation (21–23). In such applications, the deviation from steady-state magnetization as a function of slice position when using 2D cine bSSFP can potentially influence the results derived from such scans. For example, a recent study by Goldfarb et al. concluded that for late gadolinium-enhanced (LGE) imaging with 2D cine bSSFP, the end-systolic image produced the greatest difference in signal between edematous and healthy myocardial tissue (12). Although this study examined the cyclic patterns of signal deviation as a function of anatomical position within a single short axis slice containing an infarct, the degree of systolic enhancement observed may depend largely on the longitudinal position of the infarct. As another example, it has been shown that T1 measurements can be consistently lower if measured during end systole compared to end-diastole (24,25). While these studies do not explore the underlying cause of these changes, it is thought to be a result of cardiac motion and partial volume effects.

A potential method to reduce the influence of through-plane motion of the heart is to use 3D cine bSSFP, which has demonstrated similar diagnostic capacity in assessing global left ventricular structure and function to 2D cine bSSFP (26) alongside shorter overall scan time (27). However, our results reveal that while myocardial steady-state signal is well maintained regardless of longitudinal slice position when using 3D cine bSSFP, this is only valid at the center of the excited volume. Using conventional, non-accelerated 3D imaging, it was necessary to overlap the 3D slabs to such an extent that each slice was in effect acquired three times, with only one acquisition providing maintained steady-state. The deviation from steady-state as a function of position within a 3D volume, alongside increased breath-hold durations required for large 3D volumes, should be weighed when quantitative approaches necessitate properly maintained steady-state magnetization in the myocardium. However, use of accelerated imaging techniques and/or compressed sensing, or use of free-breathing imaging, could enable the acquisition of larger 3D volumes, thereby increasing the inner slab thickness in which steady-state is maintained.

One limitation to the current study was that we were unable to perform myocardial tagging or cine DENSE imaging in order to obtain accurate measurements of longitudinal displacement for each of the imaging slices. In addition, our study population was limited to only healthy individuals and did not include those with prior myocardial infarction who would demonstrate altered longitudinal shortening. Future studies that include patients with acute myocardial infarction could further probe both the role of longitudinal shortening and 3D cine bSSFP imaging for quantitative tissue characterization and perfusion imaging. Finally, we chose to use prospective gating and not retrospective triggering in order to remove the impact of heart rate on reconstructed cine frames that would be mitigated by retrospective triggering.

In conclusion, the deviation from steady-state in 2D cine bSSFP imaging is most significantly affected by the initial longitudinal position of the imaging slice within the heart. Using 3D cine bSSFP acquisitions can reduce signal fluctuations throughout the cardiac cycle as long as a sufficiently large excitation volume is used.

Declaration of conflicting interests

The author(s) declared no potential conflicts of interest with respect to the research, authorship, and/or publication of this article.

Funding

The author(s) disclosed receipt of the following financial support for the research, authorship, and/or publication of this article: This work is funded by NIH R01 HL128592-02.

References

1. Plein S, Bloomer T, Ridgway JP, et al. Steady-state free precession magnetic resonance imaging of the heart: comparison with segmented k-space gradient echo imaging. J Magn Reson Imaging 2001;14:230–236.
2. Karamitsos TD, Francis JM, Myerson S, et al. The role of cardiovascular magnetic resonance imaging in heart failure. J Am Coll Cardiol 2009;54:1407–1424.
3. Patel MR, White RD, Abbara S, et al. 2013 ACCF/ACR/ASE/ASNC/SCCT/SCMR appropriate utilization of cardiovascular imaging in heart failure. J Am Coll Cardiol 2013;61:2207–2231.
4. Kumar A, Beohar N, Arumana JM, et al. CMR imaging of edema in myocardial infarction using cine balanced steady-state free precession. JACC Cardiovasc Imaging 2011;4:1265–1273.
5. Giri S, Chung Y-C, Merchant A, et al. T2 quantification for improved detection of myocardial edema. J Cardiovasc Magn Reson 2009;11:56.
6. Stromp TA, Leung SW, Andres KN, et al. Gadolinium free cardiovascular magnetic resonance with 2-point Cine balanced steady state free precession. J Cardiovasc Magn Reson 2015;17:90.
7. Puntmann VO, Voigt T, Chen Z, et al. Native T1 mapping in differentiation of normal myocardium from diffuse disease in hypertrophic and dilated cardiomyopathy. JACC Cardiovasc Imaging 2013;6:475–484.
8. Weinsaft JW, Spincemaille P. BOLD new directions in myocardial ischemia imaging-myocardial oxygenation assessment by cardiac magnetic resonance. J Am Coll Cardiol 2012;59:1965–1967.
9. Bieri O, Scheffler K. On the origin of apparent low tissue signals in balanced SSFP. Magn Reson Med 2006;56:1067–1074.
10. Coolen BF, Heijman E, Nicholay K, et al. On the use of steady-state signal equations for 2D TrueFisp imaging. Magn Reson Imaging 2009;38:2–11.
11. Sung K, Lee H, Hu H, et al. Prediction of myocardial signal during cine balanced SSFP imaging. MAGMA 2010;23:85–91.
12. Goldfarb JW, McLaughlin J, Gray CA, et al. Cyclic CINE-balanced steady-state free precession image intensity variations: Implications for the detection of myocardial edema. J Magn Reson Imaging 2011;33:573–581.
13. De Roos A, Kundel H, Joseph P, et al. Variability of myocardial signal on magnetic resonance images. Invest Radiol 1990;25:1024–1028.
14. Jing L, Haggerty CM, Suever JD, et al. Patients with repaired tetralogy of Fallot suffer from intra-and interventricular cardiac dyssynchrony: A cardiacmagnetic resonance study. Eur Heart J Cardiovasc Imaging 2014;15:1333–1343.
15. Riffel JH, Keller MGP, Rost F, et al. Left ventricular long axis strain: a new prognosticator in non-ischemic dilated cardiomyopathy? J Cardiovasc Magn Reson 2016;18:36.
16. Buckberg G, Hoffman JIE, Mahajan A, et al. Cardiac mechanics revisited: The relationship of cardiac architecture to ventricular function. Circulation 2008;118:2571–2587.
17. Giri S, Xue H, Maiseyeu A, et al. Steady-state first-pass perfusion (SSFPP): A new approach to 3D first-pass myocardial perfusion imaging. Magn Reson Med 2014;71:133–144.
18. Jogiya R, Schuster A, Zaman A, et al. Three-dimensional balanced steady state free precession myocardial perfusion cardiovascular magnetic resonance at 3T using dual-source parallel RF transmission: initial experience. J Cardiovasc Magn Reson 2014;16:90.
19. Nguyen C, Fan Z, Sharif B. In vivo three-dimensional high resolution cardiac diffusion-weighted MRI: a motion compensated diffusion prepared balanced steady-state free precession approach. Magn Reson Med 2013;72:1257–1267.
20. Mehta BB, Auger DA, Gonzalez JA, et al. Detection of elevated right ventricular extracellular volume in pulmonary hypertension using Accelerated and Navigator-Gated Look-Locker Imaging for Cardiac T1 Estimation (ANGIE) cardiovascular magnetic resonance. J Cardiovasc Magn Reson 2015;17:110.
21. Shigenaga Y, Okajima K, Ikeuchi K, et al. Usefulness of non-contrast-enhanced MRI with two-dimensional balanced steady-state free precession for the acquisition of the pulmonary venous and left atrial anatomy pre catheter ablation of atrial fibrillation: Comparison with contrast enhanced CT in clinical cases. J Magn Reson Imaging 2016;43:495–503.
22. Renker M, Varga-Szemes A, Schoepf U, et al. A non-contrast self-navigated 3-dimensional MR technique for aortic root and vascular access route assessment in the context of transcatheter aortic valve replacement: proof of concept. Eur Radiol 2016;26:951–958.
23. Shigenaga Y, Okajima K, Ikeuichi K, et al. Acquisition of the pulmonary venous and left atrial anatomy with non-contrast-enhanced MRI for catheter ablation of atrial fibrillation: Usefullness of two-dimensional balanced staedy-state free precession. J Arrhythmia 2015;31:189–195.
24. Zhao L, Li S, Ma X, et al. Systolic MOLLI T1 mapping with heart-rate-dependent pulse sequence sampling scheme is feasible in patients with atrial fibrillation. J Cardiovasc Magn Reson 2016;18:13.

25. Ferreira VM, Wijesurendra RS, Liu A, et al. Systolic ShMOLLI myocardial T1-mapping for improved robustness to partial-volume effects and applications in tachyarrhythmias. J Cardiovasc Magn Reson 2015;17:77.
26. Peters DC, Ennis DB, Rohatgi P, et al. 3D breath-held cardiac function with projection reconstruction in steady state free precession validated using 2D cine MRI. J Magn Reson Imaging 2004;20:411–416.
27. Mascarenhas N, Muthupillai R, Cheong B, et al. Fast 3D cine steady-state free precession imaging with sensitivity encoding for assessment of left ventricular function in a single breath-hold. Am J Roentgenol 2006;187:1235–1239.